NATIONAL ADVISORY COMMITTEE
FOR AERONAUTICS

TECHNICAL NOTE 2961

SUBSONIC FLOW OF AIR THROUGH A SINGLE-STAGE

AND A SEVEN-STAGE COMPRESSOR

By Chung-Hua Wu

Lewis Flight Propulsion Laboratory
Cleveland, Ohio

NACA

Washington

June 1953
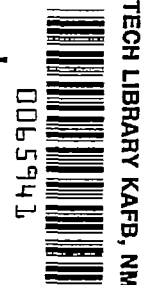
NATIONAL ADVISORY COMMITTEE FOR AERONAUTICS

TECHNICAL NOTE 2961

SUBSONIC FLOW OF AIR THROUGH A SINGLE-STAGE

AND A SEVEN-STAGE COMPRESSOR

By Chung-Hua Wu

SUMMARY

A method recently developed for solving the steady flow of a non-viscous compressible fluid along a relative stream surface between two adjacent blades in a turbomachine is applied to investigate the low- and high-speed subsonic air flow through a single-stage and through a seven-stage axial compressor. The velocity diagram used is of the "symmetrical-velocity-diagram-at-all-radii" type. The single-stage compressor has cylindrical inner and outer walls, and the multistage compressor has a cylindrical outer wall and a hub wall with an increasing radius to maintain a maximum Mach number of approximately 0.8 for all stages.

For all cases considered, converging solutions are easily obtained by the relaxation method, some of which are checked by the matrix method. Large radial flow is caused by the radially increasing values of the angular momentum of the air particles associated with this type of velocity diagram. The compressibility of the air does not change the shapes of the streamlines greatly but affects the velocity components through the increase in the density of air. The radial twist of the blade or of the stream surfaces of this type of velocity diagram has a negligible effect on the flow distribution.

In the single-stage compressor, the air moves radially inward in the inlet guide vanes and rotor and outward in the stator. The same motion occurs in the first stage of the multistage compressor, but its minimum position is moved upstream by the rising hub wall following the first rotor. The radial flow is also oscillatory throughout the rest of the multistage compressor, with a decreasing period equal to the decreasing axial length of the stages. The effect of this oscillatory radial flow is largest in the first stage, which shows a larger and a smaller negative radial gradient in the axial velocity immediately in front of and behind the rotor, respectively, than does the usual simplified-radial-equilibrium calculation, but checks very well with a simple approximation solution obtained previously for the single-stage compressor by assuming simple sinusoidal radial-flow paths.

INTRODUCTION

In the design of axial compressors that employ radially long blades, the radial variation of the state of air must be determined. For a first approximate solution, the air is assumed to be nonviscous and to flow on cylindrical surfaces that are coaxial with the axis of the machine. Solutions of the radial variation of the air state in the gap between blade rows obtained in this manner with the additional assumption of rotational symmetry are referred to as the "simple-radial-equilibrium" or "simplified-radial-equilibrium" solutions. However, even in compressors having cylindrical walls, there is considerable radial displacement of air particles across a blade row due to the compressibility of the air, the radial variation of the angular momentum of the air particles, and the radial component of blade force. The effects of the radial displacement of air particles across a blade row and of the curvature in the streamline (caused by the radial motion) on the radial distribution of air state downstream of a blade row are large (e.g., see refs. 1 to 6 for the displacement effect, and refs. 1 and 7 for the curvature effect).

In reference 1, methods are given for the solution of air state in the space between two blade rows for the limiting cases of zero and infinite blade aspect ratios. These two solutions give, respectively, the effect of radial displacement of air across the blade row and the effect of streamline curvature caused by the oscillatory displacement. For a finite aspect ratio, a simple approximate method with a simple sine curve for the shape of the streamline was suggested. In order to establish the usefulness of this simple curve for compressor designs and to investigate the detailed flow distributions in subsonic and supersonic compressors, a method based on the standard assumption of through-flow or a large number of thin blades was developed (ref. 8). The interpolation of such a solution, its modification for a finite number of thick blades, and its extension to a complete three-dimensional solution are given in reference 9.

The results obtained in applying the method developed in references 8 and 9 to a single-stage and to a seven-stage axial compressor of the "symmetrical-velocity-diagram" design are presented herein. Solutions of the inverse type are obtained for both low- and high-speed subsonic flow along a stream surface between two adjacent blades; and the effects of the compressibility of air, the radial component of blade force, and the hub contour are examined. A comparison with the approximate solution of reference 1, which assumes a simple sinusoidal streamline, is obtained by the use of the same compressor configuration and the same inlet flow for the present investigation.

SYMBOLS

The following symbols are used in this report:

B   ratio of angular thickness of stream sheet to its value
         upstream of blade row

F   vector having unit of force per unit mass of air, $F^* U_t^2 / r_t$

H   total enthalpy per unit mass of air, $h + \dfrac{V^2}{2}$; $H^* U_t^2$

h   enthalpy per unit mass of air

p   pressure of air

M   Mach number

N   nonhomogeneous term of principal equation

n   unit vector normal to stream surface

R   gas constant of air

r   radial distance, $r^* r_t$

S   relative stream surface

s   entropy per unit mass of air, $s^* R$

T   temperature of air, $T^* U_t^2 / r_t$

t   time

U   velocity of blade at radius r

V   absolute air velocity, $V^* U_t$

W   relative air velocity, $W^* U_t$

z   axial distance, $z^* r_t$

γ ratio of specific heats of air

ρ density of air

φ   angular distance measured from blade

ψ   stream function

ω   angular speed of blade

Subscripts:

a   at leading edge of inlet guide vanes

b   at trailing edge of inlet guide vanes

c   at leading edge of rotor blades or casing

d   at trailing edge of rotor blades

e   at leading edge of stator blades

f   at trailing edge of stator blades

h   hub

i   inlet to guide vanes

j   station in rotor

r, u, z   radial, tangential, and axial components

T   total state

t   at blade tip

0   refers to position where stream surface has radial element or
           where $F_r = 0$

Superscript:

*   dimensionless values

   Variables with bold partial derivative signs lie on the relative
stream surface S.

EQUATIONS GOVERNING FLOW ON RELATIVE STREAM SURFACE

BETWEEN TWO ADJACENT BLADES

A relative stream surface S about midway between two adjacent blades is shown in figure 1. The stream surface and the state of air on the surface are described by the two independent variables r and z. The steady adiabatic flow of the air along such a surface is determined by the following equations (see refs. 8 and 9):

$$\frac{\partial^2 \psi}{\partial r^2} - \frac{1}{r}\frac{\partial \psi}{\partial r} + \frac{\partial^2 \psi}{\partial z^2} = N \tag{1}$$

where

$$N = -\frac{(rB\rho)^2}{\frac{\partial \psi}{\partial r}}\left[\frac{V_u}{r}\frac{\partial(V_u r)}{\partial r} - \frac{\partial H}{\partial r} + T\frac{\partial s}{\partial r} + F_r\right] + \left(\frac{\partial \ln B\rho}{\partial r}\frac{\partial \psi}{\partial r} + \frac{\partial \ln B\rho}{\partial z}\frac{\partial \psi}{\partial z}\right)$$

$$F_u r = \frac{1}{rB\rho}\left[-\frac{\partial \psi}{\partial r}\frac{\partial(V_u r)}{\partial r} + \frac{\partial \psi}{\partial z}\frac{\partial(V_u r)}{\partial z}\right] \tag{2}$$

$$F_z = -\frac{W_u}{r}\frac{\partial(V_u r)}{\partial z} - T\frac{\partial s}{\partial z} + \frac{\frac{\partial \psi}{\partial z}}{\frac{\partial \psi}{\partial r}}\left[\frac{\partial H}{\partial r} - \omega\frac{\partial(V_u r)}{\partial r}\right] -$$

$$\frac{1}{(rB\rho)^2}\frac{\partial \psi}{\partial z} \times \left[\frac{\partial^2 \psi}{\partial r^2} - \frac{1}{r}\frac{\partial \psi}{\partial r} + \frac{\partial^2 \psi}{\partial z^2} - \frac{1}{B\rho}\left(\frac{\partial \psi}{\partial r}\frac{\partial B\rho}{\partial r} + \frac{\partial \psi}{\partial z}\frac{\partial B\rho}{\partial z}\right)\right] \tag{3}$$

$$F_r = F_u r \int_{z_0}^{z} \frac{\partial}{\partial r}\left(\frac{F_z}{F_u r}\right) dz \tag{4}$$

$$\frac{\rho}{\rho_{T,i}} = \left[\frac{H}{H_i} - \frac{(V_u r)^2}{2H_i r^2} - \frac{\left(\frac{\partial \psi}{\partial r}\right)^2 + \left(\frac{\partial \psi}{\partial z}\right)^2}{2H_i(rB\rho)^2}\right]^{\frac{1}{\gamma-1}} e^{s_{T,i}-s} \tag{5}$$

$$\frac{DH}{Dt} = \omega\frac{D(V_u r)}{Dt} \tag{6}$$

Equations (1) to (3) are the equations of motion in the radial, cir-
cumferential, and axial directions, respectively; equation (4) repre-
sents the integrable condition of the stream surface; equation (5)
is obtained from the thermodynamic relation among density, enthalpy,
and entropy; and equation (6) is derived from the condition that the
vector F is normal to the stream surface and the equation of motion
(see ref. 8). In these equations, the bold partial derivative signs
emphasize the fact that the variables are those lying on the relative
stream surface S.

In the present investigation, the inlet flow considered is uniform
in H and s. For the symmetrical velocity diagram chosen $\partial H/\partial r$ is
then equal to zero everywhere. In the calculations for the single-stage
compressor, no entropy change is considered. For the multistage compres-
sor, however, an estimated entropy increase in the z-direction (but uni-
form radially) corresponding to a polytropic efficiency of 0.9 at the
mean blade height is used, in order to use the same hub contour calcu-
lated on that basis in reference 9.

The variable B can be considered as the ratio of the local angu-
lar thickness of a stream sheet (whose mean surface is the stream sur-
face S of fig. 1) to its value at the inlet to the blade row, and is
closely related to the variation in the angular thickness of the blades.
A given variation of B specified in the design calculation will lead
to a particular blade-thickness variation when a complete three-
dimensional inverse solution is carried out. Since the purpose of the
present investigation is to study only the effects of the compressi-
bility of air, the radial variation of the angular momentum of air
particles, the radial component of blade force, and the noncylindrical
hub-wall shape on the flow distribution, B is assumed, for simplicity,
equal to a constant 1 everywhere. Hence, the solutions obtained closely
represent those in compressors in which thin blades are used. The solu-
tion, of course, becomes exact for the limiting case of infinite number
of blades of zero thickness.

The vector F, which is, in general, defined by

$$F = - \frac{1}{n_u r}\left(\frac{\partial h}{\partial \varphi} - T\,\frac{\partial s}{\partial \varphi}\right) n = -\frac{1}{n_u r}\frac{1}{\rho}\frac{\partial p}{\partial \varphi}\, n \qquad (7)$$

gives the effect of the circumferential pressure gradient at the mean
stream surface for the variation of tangential velocity prescribed on
it. In the limiting case of an infinite number of blades of zero thick-
ness, F becomes simply the blade force.

SINGLE-STAGE COMPRESSOR

Prescribed Conditions

The compressor design chosen employs symmetrical velocity diagrams at all radii and a radially constant total enthalpy. In addition, the following conditions are specified in the design calculation: hub and casing shapes, blade aspect ratio, axial rate of change of $V_u r$ on the mean stream surface, and position of the radial element of the mean stream surface. The shape of the mean stream surface is to be determined after the solution of the flow variation on it is obtained.

In order to compare results herein with those obtained in reference 1, similar inlet flow conditions, hub and casing shapes, blade-row aspect ratio, and rotor speed are used in the present investigation (see fig. 2). The hub and casing walls are cylindrical surfaces coaxial with the machine axis; the hub-to-casing radius ratio is 0.6; the blade aspect ratio (based on axial blade length) is 2.67 (which corresponds to the blade-row aspect ratio of 2 used in ref. 1); and the ratio of inlet velocity to rotor tip speed is 0.7378. In addition, a stator is added downstream of the rotor to give the angular momentum of the air particles downstream of the stator the same value as that entering the rotor.

When generalized for compressible flow with radial displacement across the blade row, the symmetrical-velocity-diagram-at-all-radii is defined on the mean stream surface by the following equation (see fig. 2 and p. 10 of ref. 1):

$$\frac{\partial (V_u r)_b}{\partial r_b} + \frac{\partial (V_u r)_e}{\partial r_b} = 2\omega r_b \tag{8}$$

In order that, for any fixed value of z, the total enthalpy of air on the stream surface be constant with respect to the radius, that is, $\partial H/\partial r = 0$, the variation of $V_u r$ on the stream surface is such that the same amount of work is done on the air along all streamlines between the exit station of the inlet guide vanes (station b) and a station j in the rotor (fig. 2). Thus, along a streamline,

$$(V_u r)_j - (V_u r)_b = f(z_j) = \left[(V_u r)_j - (V_u r)_b \right]_t \tag{9}$$

Hence,

$$\frac{\partial (V_u r)_j}{\partial r_b} - \frac{\partial (V_u r)_b}{\partial r_b} = 0 \tag{10}$$

Combining equations (8) and (10) gives

$$\frac{\partial (V_u r)_j}{\partial r_b} = \omega r_b \tag{11}$$

Therefore, from equations (8) and (9)

$$(V_u r)_b = \frac{\omega r_b{}^2}{2} - \frac{(V_u r)_{e,t} - (V_u r)_{b,t}}{2} \tag{12}$$

$$(V_u r)_e = \frac{\omega r_b{}^2}{2} + \frac{(V_u r)_{e,t} - (V_u r)_{b,t}}{2} \tag{13}$$

and

$$(V_u r)_j = (V_u r)_b + \left[(V_u r)_{j,t} - (V_u r)_{b,t}\right] \tag{14}$$

The specified variation of $f(z)$ or $\left[(V_u r) - (V_u r)_b\right]_t$ in the rotor is shown in figure 3. A constant rate of change in $V_u r$ is maintained for the first half of the rotor blade, and a rate linearly decreasing to zero is used for the second half. Taken from reference 1, the values of $V_u r$ (after division by $U_t r_t$) at the inlet to the rotor and leaving the rotor are, respectively, 0.32161 and 0.67840 at the casing.

Similar rates of change of $V_u r$ with respect to z are prescribed for the inlet guide vanes and the stator. For the inlet guide vanes, $V_u r$ changes from the initial value of zero at the inlet to that given by equation (12) at station b. For the stator, the value of $V_u r$ is changed from the value at station e (same as that obtained at station d) to a value at station f equal to that at station b.

Method of Solution

Solution of the present investigation is obtained by the general method of successive approximation. Equation (1) is taken as the principal equation to be solved. The last two terms in the equation are calculated by the use of equations (2) to (6) and of the flow variations obtained in the preceding cycle (see ref. 10). One additional complication in the present calculation is that the value of $V_u r$ at

any station in the rotor and stator as given by equation (14) requires knowledge of the radial variation of the stream function at station b. A plot of ψ_b as a function of r_b is first made. From the value of stream function at a grid point j in question (either in the rotor or the stator), the value of r_b corresponding to the same streamline is read from the plot.

In the present investigation, solutions for the four cases considered are obtained by the relaxation method in the manner described in reference 10 and are checked by the matrix method with the same matrix factors (extended to include an extra blade length) given in reference 10. Much quicker convergence is obtained in the present calculation than in reference 10, because of the predominant influence of the specified variation of $V_u r$ and the very small magnitude of F_r. The values of stream function obtained by the matrix method, in general, agree very well with those obtained by the relaxation method.

In the calculation, all quantities are rendered dimensionless in the same manner as in reference 10. That is, r or z, V or W, ρ, T, s, H, F, ψ, and ω are divided, respectively, by r_t, U_t, $\rho_{T,i}$, U_t^2/R, R, U_t^2, U_t^2/r_t, $\rho_{T,i}U_t r_t^2$, and U_t/r_t. These dimensionless quantities are denoted by the superscript $*$.

A zero value of ψ is chosen at the hub. For the chosen conditions of $V_i^* = 0.7378$ and $H_i^* = 4.5736$ (which correspond to the solution of ref. 1), $\rho_i^* = 0.8578$, $M_i = 0.56$, and $\psi_c^* = \frac{1}{2} \rho_i^* V_i^* (1 - r_h^{*2}) = 0.20252$. This ψ value at the casing is also used in the incompressible solution.

As in reference 10, an inlet station is chosen at $z^* = -0.525$, at which ψ increases radially with the square of radius. This simple variation results from the fact that, with no tangential and radial components of velocity and with radially uniform values of H and s, the axial velocity and density are also radially uniform. At the last station downstream of the stator ($z^* = 1.20$), however, the tangential velocity is not equal to zero, and both the axial velocity and density are radially nonuniform. At the beginning of computation, an approximate radial variation there is determined on a radial variation of tangential velocity computed according to equation (12), and the radial variations of axial velocity and density are computed by the use of, respectively, equations (D13) and (D14) of reference 1. These ψ values are corrected in successive cycles on the condition that they become uniform in z-direction when V_r and its rate of change approach zero far downstream of the last blade row.

RESULTS AND DISCUSSION

For adiabatic flow of a nonviscous air with uniform entropy s and
enthalpy H at the inlet to the machine and the chosen design specifi-
cations, the deviation of air flow from that on a cylindrical surface
is due to three factors: (1) the specified radial variation of the
angular momentum of the air particles $V_u r$; (2) the radial component
of F; and (3) the compressibility of air (see eq. (1) for the expres-
sion of the nonhomogeneous term N). In order to study the relative
importance of these three factors on the flow distribution, the follow-
ing four cases are considered:

    I. Incompressible solution neglecting F_r

    II. Compressible solution neglecting F_r

    III. Incompressible solution including F_r

    IV. Compressible solution including F_r

Incompressible solution neglecting F_r (case I). - Case I is cal-
culated in order to show the effect of the specified "nonvortex" varia-
tion of the angular momentum of air particles on the flow distribution.
The nonhomogeneous term N of the principal equation (1) is roughly
equal to, in the present case,

$$N \approx - \omega \rho_i \frac{V_u r}{V_z}$$

Hence, N is always negative and its magnitude varies in the z-direction
roughly with $V_u r$ (see fig. 2). This distribution of N requires a
general increase in ψ from the inlet value for a given radius every-
where in the flow region except on the inner and outer walls. The maxi-
mum increase occurs at z^* equal to about 0.375. (Compare case C of
ref. 10 for similar N and ψ distributions in the rotor and the
stator.) The shapes of the streamlines, which divide the total mass
flow into ten equal parts, are shown in figure 2. Corresponding to
increasing value of tangential velocity through the inlet guide vanes
and the rotor (fig. 3), the air flows radially inward in the inlet
guide vanes and the rotor. It then flows radially outward in the stator,
corresponding to a decreasing value of tangential velocity there. If
there are similar stages following the stator, the air will repeat this
flow pattern for each stage, that is, radially inward in the rotor and
radially outward in the stator. The shape of the streamlines indicates
that they can be approximated by simple sinusoidal curves for each
stage as suggested in reference 1. The shape of the relative stream
surfaces in the inlet guide vanes, rotor, and stator is indicated in
figure 4.

Figure 5 shows the variations of the tangential velocity with respect to z at several radii obtained in the solution. They are seen to be quite similar to the specified variation at the casing, because the difference between r_b and r is less than 1 percent of r. The radial variation of V_u is very similar to that in a simplified-radial-equilibrium calculation.

The axial and radial velocity distributions are computed by the use of the following equations:

$$V_z = \frac{1}{\rho r} \frac{\partial \psi}{\partial r} \qquad (15)$$

$$V_r = - \frac{1}{\rho r} \frac{\partial \psi}{\partial z} \qquad (16)$$

The variations of axial and radial velocity with respect to z at several radii are shown in figures 6 and 7. The magnitude of the axial velocity is inversely proportional to the distance between the streamlines shown in figure 2. The largest radial variation in axial velocity is located in the space between the rotor and the stator.

The variation in radial velocity shown in figure 7 corresponds to the variation of axial velocity and the slope of the streamline. The radial velocity does not vanish for more than 2 axial-chord distances upstream of the inlet guide vanes and downstream of the stator. The partial derivative of V_r with respect to z is negative at z^* equal to 0.175 (midway between the inlet guide vanes and the rotor) and is positive at z^* equal to 0.375 (midway between the rotor and the stator). Although the radial displacement of the streamline and the radial velocity are relatively small, it is the gradient in radial velocity that significantly affects the radial distribution of the axial velocity (see fig. 12 to be discussed later and ref. 1).

Compressible solution neglecting F_r (case II). - In case II, the nonhomogeneous term N of the principal equation (1) has an additional term accounting for the variations of density. This additional term is always positive in the blade region for the chosen configuration. Its magnitude is initially of the same order as the first term, which contains $\partial(V_u r)/\partial r$, but falls to about 1 percent of this first term at $z^* = 0.55$. The first term in this case for regions behind the rotor blade has a much greater magnitude than the first term in case I because of the increasing value of density (note that it is multiplied by the square of density).

The magnitudes of the nonhomogeneous term for cases I and II at the radius r_t of 0.8 are compared in table I, which shows that for z^* greater than 0.25, the magnitude of N in case II is larger than that in case I. As a result, the streamlines in the region of rotor and stator obtained in case II lie below those of case I.

The variation of density obtained in the solution is shown in figure 8. The density decreases slightly through the inlet guide vanes. It then increases continuously in the rotor and the stator. At the exit of the rotor, it is higher at the tip than at the root. At the exit of the stator, however, ρ^* varies only slightly from 1.09 to 1.10 from hub to casing. The static pressure there is similarly uniform.

Because the partial derivative of ψ with respect to the radius is only slightly changed from case I to case II, this variation of density in case II gives an axial velocity (fig. 6) somewhat greater than that in case I in the guide vanes but increasingly smaller in the rotor and the stator (see eqs. (15) and (16)). Radially, the axial velocity still decreases from hub to casing.

The variation of radial velocity obtained in this case is, in general, similar to that of case I. In the rotor, the magnitude of the radial velocity is larger; while in the stator, the magnitude is smaller. This difference between the two cases is mainly due to the difference in the streamlines.

The values of tangential velocity in cases I and II are different only up to 1 percent and cannot be shown with the scale used in figure 5.

Effect of F_r (cases III and IV). - The effects of F_r on the flow distribution are investigated for both incompressible and compressible flow by computing F_r according to equations (2) to (4) and including it in the nonhomogeneous term N in the solution of the principal equation (1). The variations of the three components of F are shown in figures 9 to 11. It is seen that the magnitude of F_r is rather small. The maximum magnitude in the dimensionless form is only 0.2 compared with a maximum magnitude of 3 in a gas turbine (case D of ref. 10). In the present cases, F_r is significant only at the leading edge of the rotor blades at hub and tip, where the influence on the flow is relatively small. At most other places, F_r is less than 5 percent of $V_u r \times \partial(V_u r)/\partial r$. With this relatively large effect of the radial variation of the angular momentum of the air particles, it is expected that the flow distribution will be only slightly affected by the inclusion of the F_r term. This small effect is evident from tables I and II, where the variations of the nonhomogeneous term N and the stream function ψ at r^* equal to 0.8 obtained by the matrix method are

compared. The difference in N between case I (incompressible solution neglecting F_r) and case III (incompressible solution considering F_r) and that between case II (compressible solution neglecting F_r) and case IV (compressible solution considering F_r) are in general very small (table I). The variations of ψ obtained in cases III and IV are very much the same as those in cases I and II, respectively, (table II); and the magnitude is different by no more than 0.2 percent in most places, with a maximum of 0.5 percent at z^* equal to zero. With this similar variation in ψ and very small difference in the magnitude, the derivatives of ψ and the corresponding velocity components and density of air (see eqs. (15), (16), and (5)) are, in general, even less different between cases I and III and II and IV, respectively. The results shown previously for cases I and III (figs. 2 to 8) can therefore be taken as those of cases II and IV, respectively, without appreciable error.

Radial variation of axial velocity in front of rotor and stator. The radial variations of axial velocity obtained in the incompressible and compressible solutions at z^* equal to 0.175 and 0.375 are shown in figure 12. The variations obtained in reference 1 for the simplified-radial-equilibrium calculation, for the limiting cases of zero and infinite aspect ratio, and for the same blade aspect ratio of 2.67 based on an assumed sinusoidal streamline (all for compressible flow) are also shown for comparison. (These values at the second station, $z^* = 0.375$, are recomputed for 100-percent efficiency.) The incompressible solution gives a good indication in the gradient of the radial variation of axial velocity; but it gives a smaller value in the gap between the inlet guide vanes and the rotor, and a much too great value in the gap between the rotor and the stator because of the neglect of the decrease of density of air in passing through the guide vanes and in the increase of density of air in passing through the rotor.

For the compressible solutions, an approximate solution based on a simple sinusoidal curve for the projection of a streamline in the meridional plane gives a very good approximate value, especially in the gap between rotor and stator. This good agreement is to be expected from the shapes of the streamlines shown in figure 4. For compressors employing other similar types of velocity diagram, it may be expected that the simple approximate method suggested in reference 1 would also give good approximate answers. The limiting solutions of zero and infinite aspect ratio give values enveloping the solution of the blade aspect ratio of 2.67.

The simplified-radial calculation is seen to give a smaller negative gradient at z^* equal to 0.175 and a much too large negative gradient at z^* equal to 0.375. An error in the axial velocity determination, of course, will give error in blade angle, Mach number, optimum rotor speed, and so forth. For example, at the tip, the relative rotor-blade discharge angle should be 37.5°. Simplified-radial-equilibrium assumption would give 43°, an error of 5.5°.

SEVEN-STAGE COMPRESSOR

Prescribed Conditions

In order to investigate the oscillating nature of radial flow in a multistage compressor and the effect of the rising hub-wall radius on the flow, similar computation is made for a seven-stage compressor. The compressor configuration chosen is the typical one investigated in reference 11, (see appendix and figs. 9 to 11 of that ref.). It has an inlet hub-tip radius ratio of 0.5 and a design specific mass flow of 30 pounds per second per square foot of frontal area at an equivalent rotor tip speed of 815 feet per second. The velocity diagram used is the same as that used in the single-stage calculation. The hub contour was determined by an approximate method for a maximum Mach number of 0.8 for all stages. The axial length of blade is determined for a constant Reynolds number of 8×10^5 at sea level or 2×10^5 at an altitude of 35,000 feet, and a tip radius of 1 foot (fig. 13).

The ratio of inlet velocity to rotor tip speed is 0.74433; the inlet Mach number is 0.56; and the dimensionless stream function at casing ψ_c^* is equal to 0.23971 with the value at hub chosen to be zero.

The prescribed values of the tangential velocity at the exit of the inlet guide vanes and stators as determined in reference 11 are shown in figure 14. The specified variation of $V_u r$ along z in the inlet guide vanes is such that a constant rate of change is maintained for four-sevenths of the blade length and a rate linearly decreasing to zero for the remaining portion. In the rotors, in order that the total enthalpy of air be radially constant, the variation of $V_u r$ follows the procedure discussed before for the single-stage compressor, the only difference being that the variation specified along the casing has a constant rate until four-sevenths of the blade length instead of one-half. (This point of transition is chosen, because each blade is spanned axially by eight grid points in the numerical solution.) The stator then changes the tangential velocity at the exit of the rotor to the specified value at the exit of stator blade in a similar manner.

Method of Solution

The solution of this seven-stage compressor is similar to that described for the single-stage compressor. The only additional difficulty lies in the curved hub boundary and the decreasing axial blade length along the flow path. This difficulty is solved by the use of the tables and formulas of numerical differentiation coefficients given in reference 10. The regular grid distance in the radial direction is chosen as 0.0625, which gives in the radial direction nine grid points

for the first three blades and three grid points for the last three
blades. The grid size in the axial direction decreases with the stage
length in such a manner that there are always eight equally spaced sta-
tions across each blade and one station in the gap between two blades.
Radially, then, either equally spaced grids or one unequal spacing at
the lower end is involved and the corresponding differentiation coef-
ficients based on either second- or fourth-degree polynomial are avail-
able in the tables of reference 12. Axially, however, several unequal
spacings are involved in many places if the fourth-degree formulas are
used. The present solution is obtained by the relaxation method with
a desk calculator and by the use of these calculated coefficients kept
to a maximum of six figures. Experience gained in the single-stage
compressor and this problem indicates that with the chosen grid size
(especially in the axial direction) a three-point formula would have
given sufficient accuracy.

Because the effect of F_r is found negligible for this type of
blading, F_r is not included in the solution, and only equations (1),
(5), (6) are involved in the present calculation. To correspond to the
calculation made in reference 11, an increase of entropy axially is
computed for a polytropic efficiency of 0.9 at approximately midblade
height (uniform radially) to account for the effect of viscous loss on
the density increase (through eq. (5)) and thereby the velocities
(through eqs. (15) and (16)).

Figure 13 shows the meridional projection of the streamlines
obtained in the compressible solution. A close examination on a much
larger plot and the numerical values obtained in the solution show the
following:

(1) The shape of the streamline consists of an oscillatory compo-
nent superposed on a mean line which follows the general shape of the
hub walls.

(2) In the inlet guide vanes and the first rotor, the air flows
radially inward and (because of the rising hub wall radius downstream
of the rotor) begins to flow radially outward before it leaves the
rotor. At the exit of the rotor, however, the radial position is still
considerably lower than that entering the guide vanes.

(3) The air continues to flow radially outward in the first stator.
At the exit of the stator, its radial position is still lower than that
computed on the basis that the specific mass flow across the annulus
area is radially uniform.

(4) In the second stage, consisting of the second rotor and the
second stator, the radial position of the streamlines first moves

farther outward and then toward a straight line which passes through the radial position of the projected streamline immediately upstream and downstream of the stage. This shape is similar to that of the hub contour at that stage. The streamlines still lie below the geometrical lines computed on the simple area basis.

(5) The oscillatory component of the projected streamline decreases its magnitude as the air moves downstream to the short-blade region.

CONCLUSIONS

From the solutions obtained for the low- and high-speed subsonic flow through a single- and a seven-stage compressor of the symmetrical-velocity-diagram design, the following conclusions are made:

1. The radially increasing angular momentum of the air particles associated with this type of design and the curved hub wall contour have the predominating influence on the flow distribution.

2. The compressibility of the air does not change the shapes of the streamlines greatly but exerts its influence mostly through the increase of the air density in the calculation of the velocity components according to the streamline distributions.

3. The effect on the flow distribution of the small amount of radial twist of this type of blading is negligible.

4. In general, the air moves radially inward through the inlet guide vanes and the first rotor and then radially outward in the first stator.

5. Oscillatory radial flow continues throughout the compressor with a period equal to the length of the stage.

6. The effect of this oscillatory radial flow is largest in the first stage (inlet stage) of a multistage compressor. The radial position of an air particle in the stage is much lower than the value computed on the basis of a radially uniform specific mass flow and its position at the inlet to the machine. The negative radial gradient in the axial velocity of the air immediately upstream of the first rotor and the first stator is, respectively, larger and smaller than the simplified-radial-equilibrium solution, but checks very well with the simple approximate solution obtained previously for the single-stage compressor by assuming simple sinusoidal radial-flow paths.

Lewis Flight Propulsion Laboratory
    National Advisory Committee for Aeronautics
        Cleveland, Ohio, March 13, 1953

REFERENCES

1. Wu, Chung-Hua, and Wolfenstein, Lincoln: Application of Radial-
   Equilibrium Condition to Axial-Flow Compressor and Turbine Design.
   NACA Rep. 955, 1950. (Supersedes NACA TN 1795.)

2. Kahane, A.: Investigation of Axial-Flow Fan and Compressor Rotors
   Designed for Three-Dimensional Flow. NACA TN 1652, 1948.

3. Marble, Frank E.: The Flow of a Perfect Fluid Through an Axial
   Turbomachine with Prescribed Blade Loading. Jour. Aero. Sci.,
   vol. 15, no. 8, Aug. 1948, pp. 473-485.

4. Bowen, J. T., Sabersky, R. H., and Rannie, W. D.: Investigations of
   Axial-Flow Compressors. A.S.M.E. Trans., vol. 73, no. 1, Jan. 1951,
   pp. 1-14.

5. Bragg, Stephen L., and Hawthorne, William R.: Some Exact Solutions
   of the Flow Through Annular Cascade Actuator Discs. Jour. Aero.
   Sci., vol. 17, no. 4, Apr. 1950, pp. 243-249.

6. Siestrunck, R., et Fabri, J.: Écoulements tourbillonnaires dans
   les machines axiales. Office National d'Études et de Recherches
   Aeronautiques. Pub. 45, 1950.

7. Marble, Frank E.: Some Problems Concerning the Three-Dimensional
   Flow in Axial Turbomachines. Preprint No. 182, Inst. Aero. Sci.,
   1949.

8. Wu, Chung-Hua: A General Through-Flow Theory of Fluid Flow with
   Subsonic or Supersonic Velocity in Turbomachines of Arbitrary Hub
   and Casing Shapes. NACA TN 2302, 1951.

9. Wu, Chung-Hua: A General Theory of Three-Dimensional Flow in Sub-
   sonic and Supersonic Turbomachines of Axial-, Radial-, and Mixed-
   Flow Types. NACA TN 2604, 1952.

10. Wu, Chung-Hua: Matrix and Relaxation Solutions That Determine
    Subsonic Through Flow in an Axial-Flow Gas Turbine. NACA TN
    2750, 1952.

11. Wu, Chung-Hua, Sinnette, John T., Jr., and Forrette, Robert E.:
    Theoretical Effect of Inlet Hub-Tip-Radius Ratio and Design
    Specific Mass Flow on Design Performance of Axial-Flow Compres-
    sors. NACA TN 2068, 1950.

12. Wu, Chung-Hua: Formulas and Tables of Coefficients for Numerical
    Differentiation with Function Values Given at Unequally Spaced
    Points and Application to Solution of Partial Differential Equa-
    tions. NACA TN 2214, 1950.

TABLE I. - COMPARISON OF NONHOMOGENEOUS

TERM N* AT r* = 0.8 IN PRINCIPAL

EQUATION FOR FOUR CASES CONSIDERED

z*	Case			
	I	II	III	IV
0	0	0.018240	-0.007214	0.008976
.05	-.034858	-.014352	-.037363	-.004704
.10	-.066619	-.050880	-.059448	-.022320
.15	-.077942	-.056208	-.078696	-.055440
.20	-.078749	-.035232	-.077693	-.026448
.25	-.166790	-.160512	-.161928	-.145440
.30	-.247531	-.284832	-.265546	-.303504
.35	-.277210	-.325728	-.277579	-.330432
.40	-.276941	-.331200	-.276658	-.306048
.45	-.188827	-.287376	-.183974	-.273696
.50	-.108082	-.176400	-.125338	-.200832
.55	-.078115	-.125568	-.077506	-.132624

TABLE II. - COMPARISON OF ψ* AT r* = 0.8 OBTAINED BY

MATRIX METHOD FOR FOUR CASES CONSIDERED

z*	Case			
	I	II	III	IV
0	0.089147	0.089277	0.089660	0.089151
.05	.089801	.089730	.090161	.089538
.10	.090597	.090419	.090834	.090125
.15	.091476	.091280	.091618	.090944
.20	.092389	.092245	.092491	.091963
.25	.093382	.093402	.093472	.093168
.30	.094498	.094889	.094606	.094721
.35	.095451	.096319	.095603	.096244
.40	.095928	.097228	.096061	.097153
.45	.095805	.097486	.095914	.097367
.50	.095134	.097117	.095249	.097044
.55	.094260	.096336	.094409	.096366
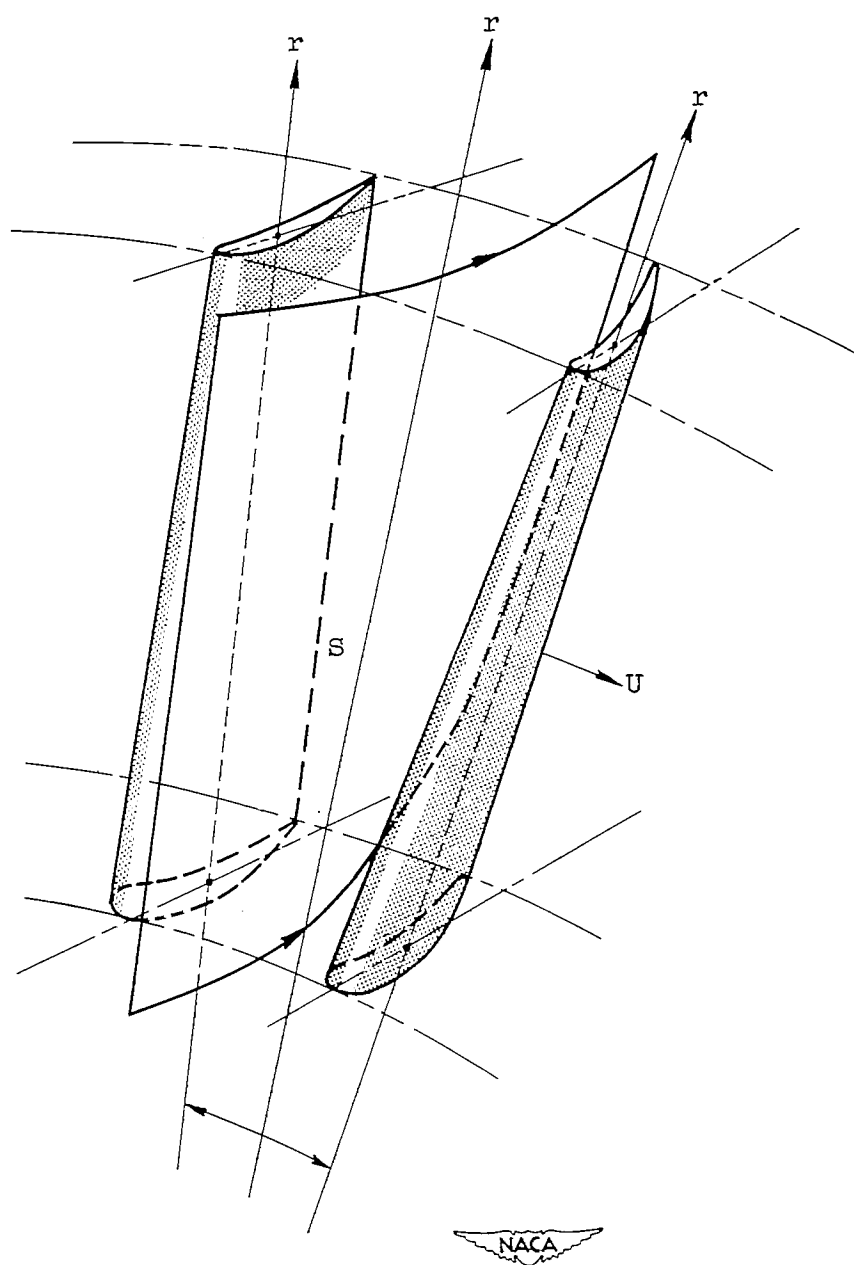
Figure 1. - Relative stream surface midway between two adjacent blades.
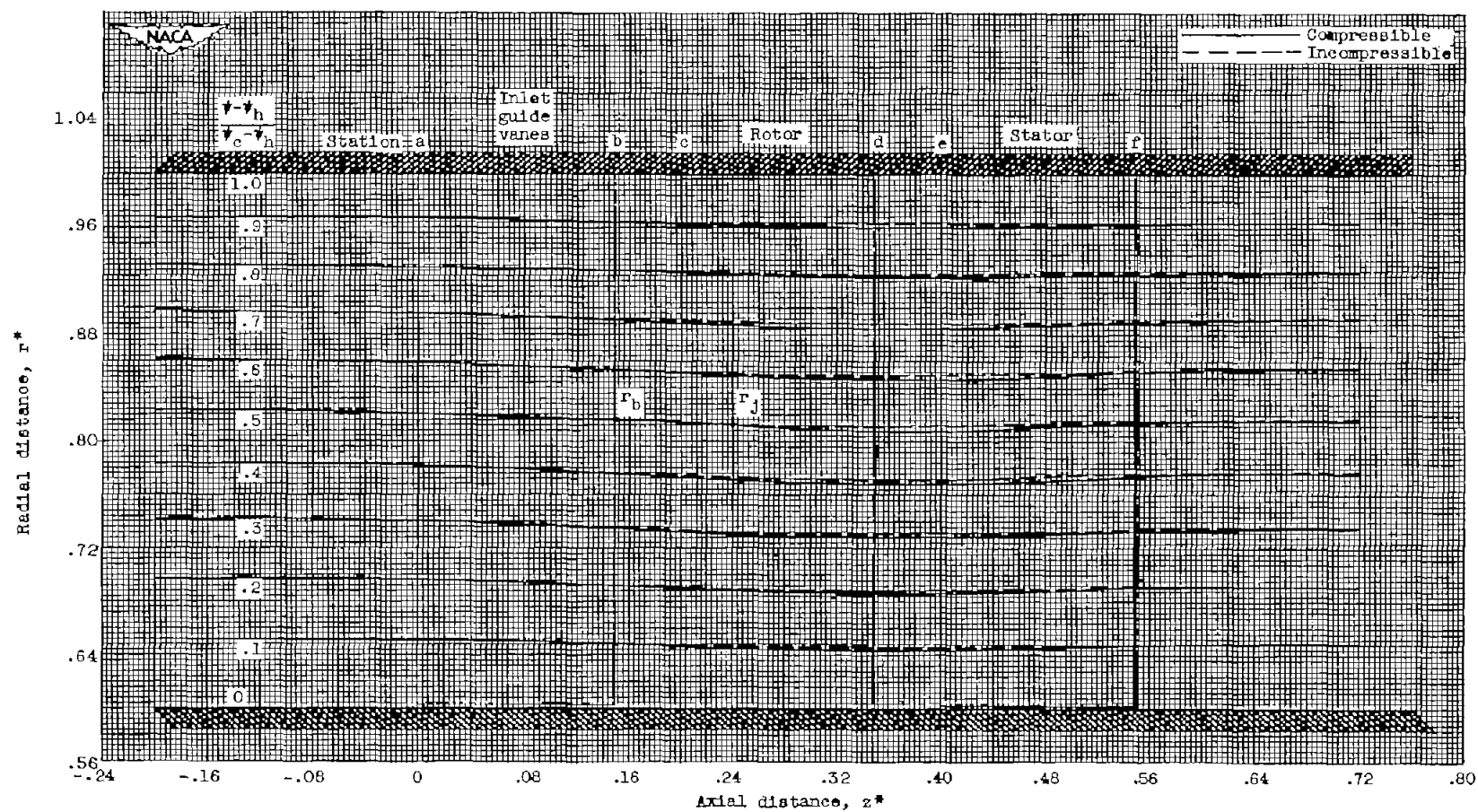
Figure 2. - Meridional section of single-stage compressor and meridional projection of streamlines.
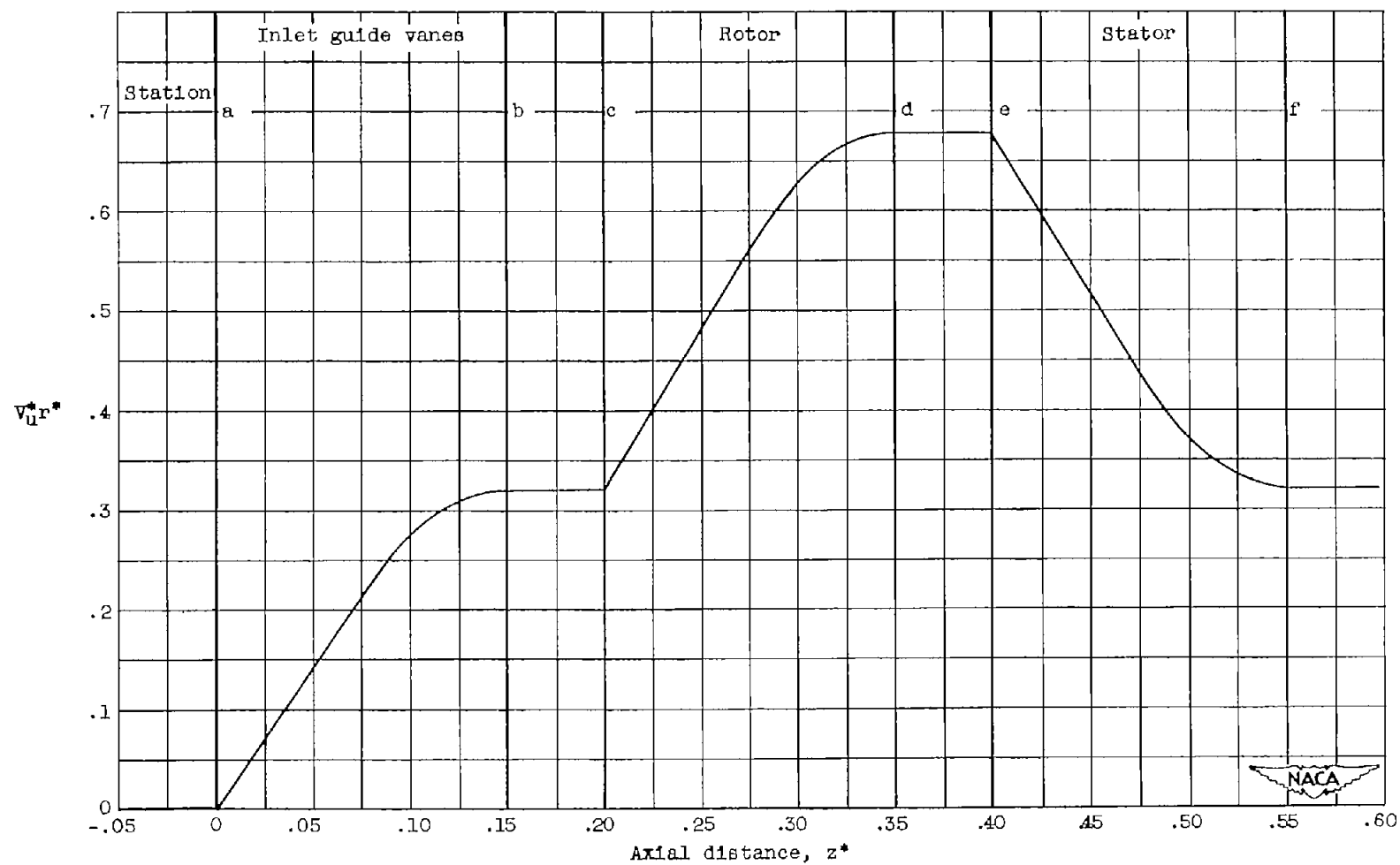
Figure 3. - Prescribed variation of tangential velocity along casing.
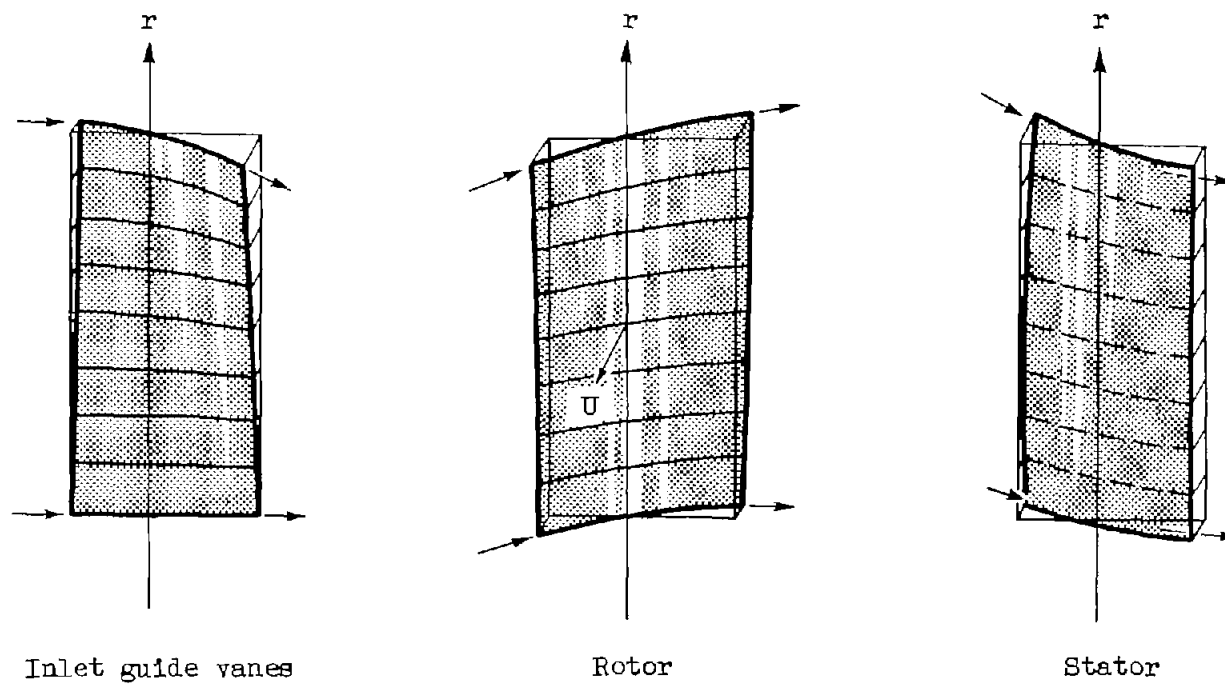
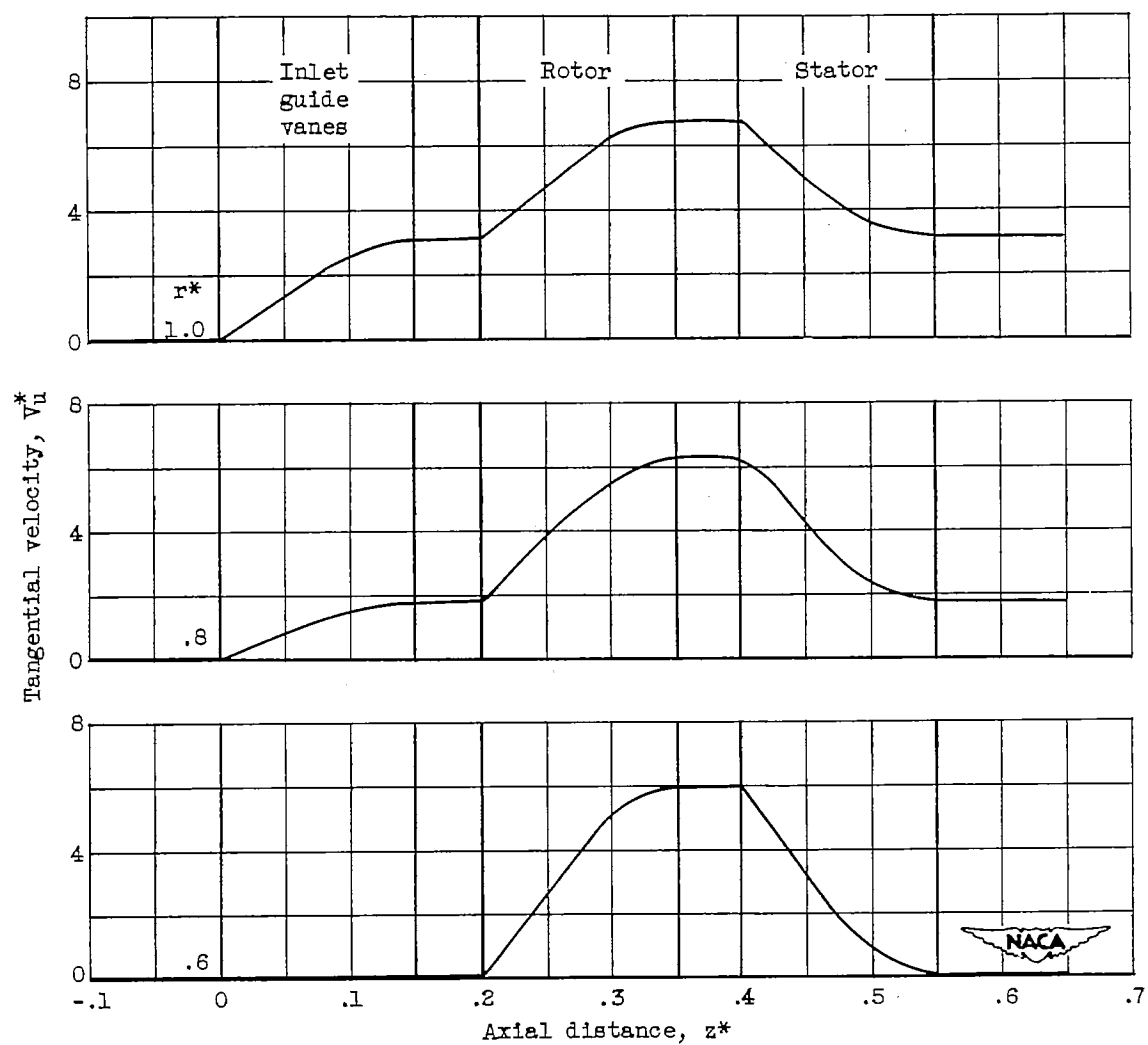Figure 4. - Relative stream surfaces in inlet guide vanes, rotor, and stator.
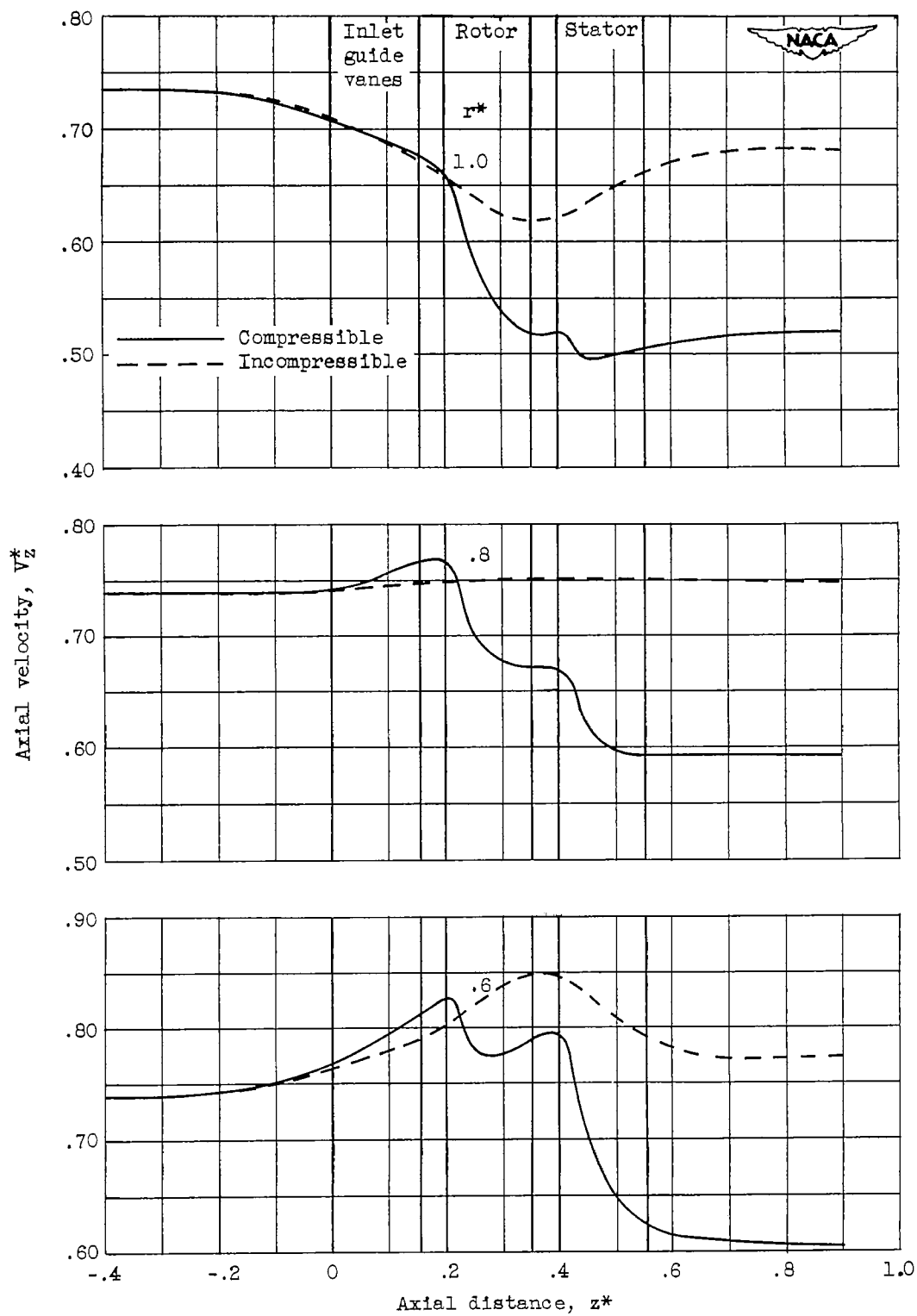
2519

Figure 5. - Variation of tangential velocity.
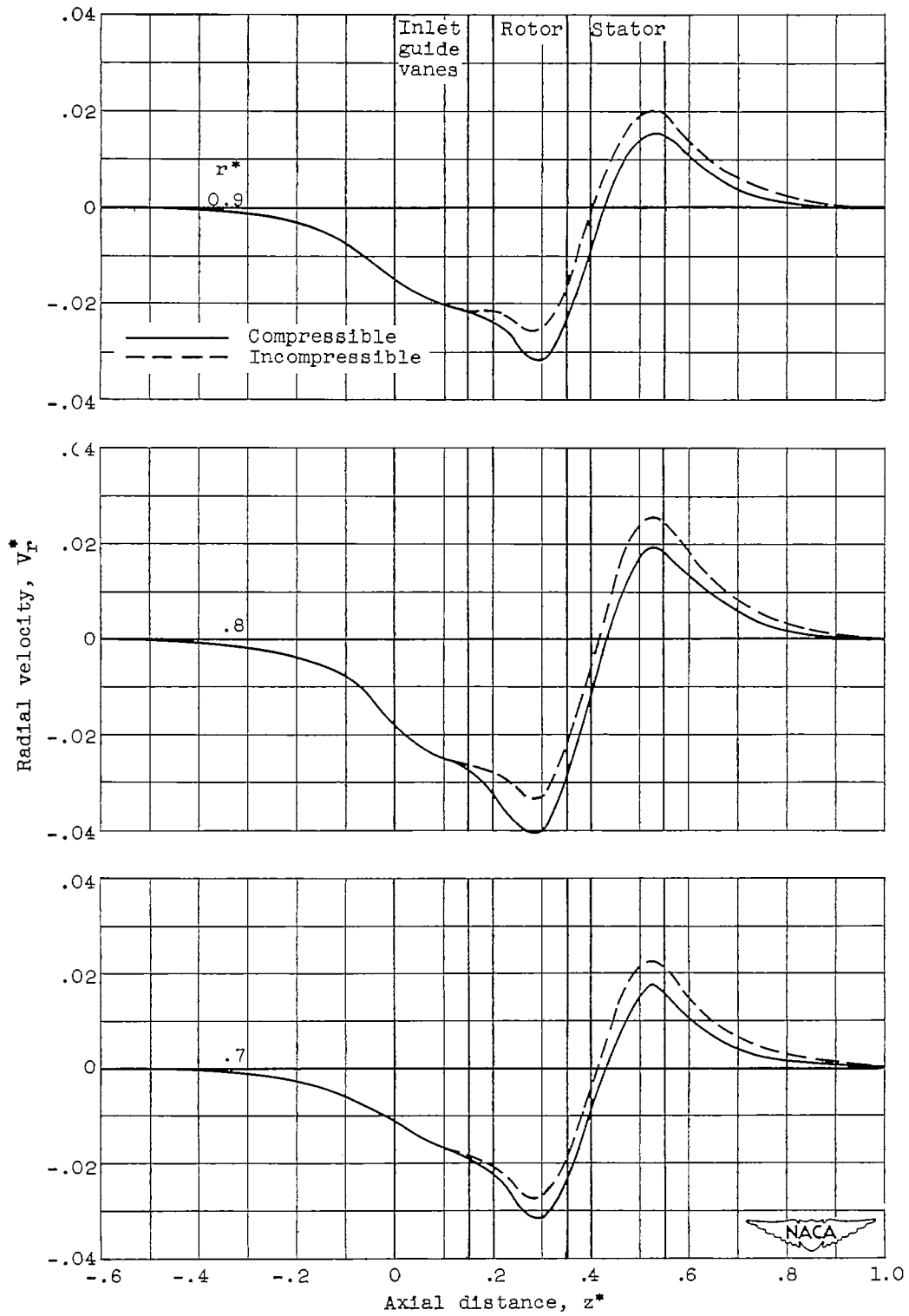
Figure 6. - Variation of axial velocity.
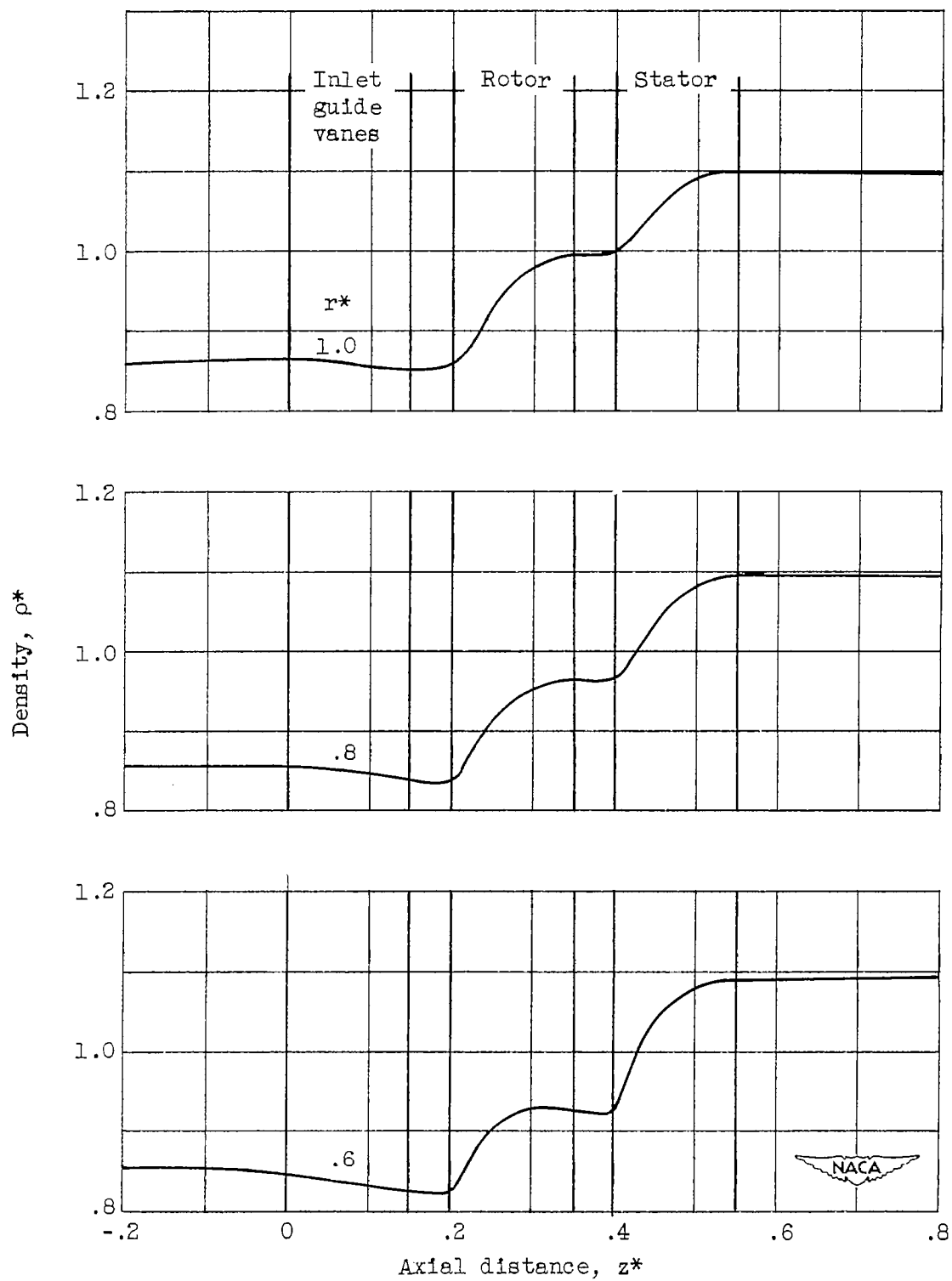
Figure 7. - Variation of radial velocity.

Figure 8. - Variation of density.
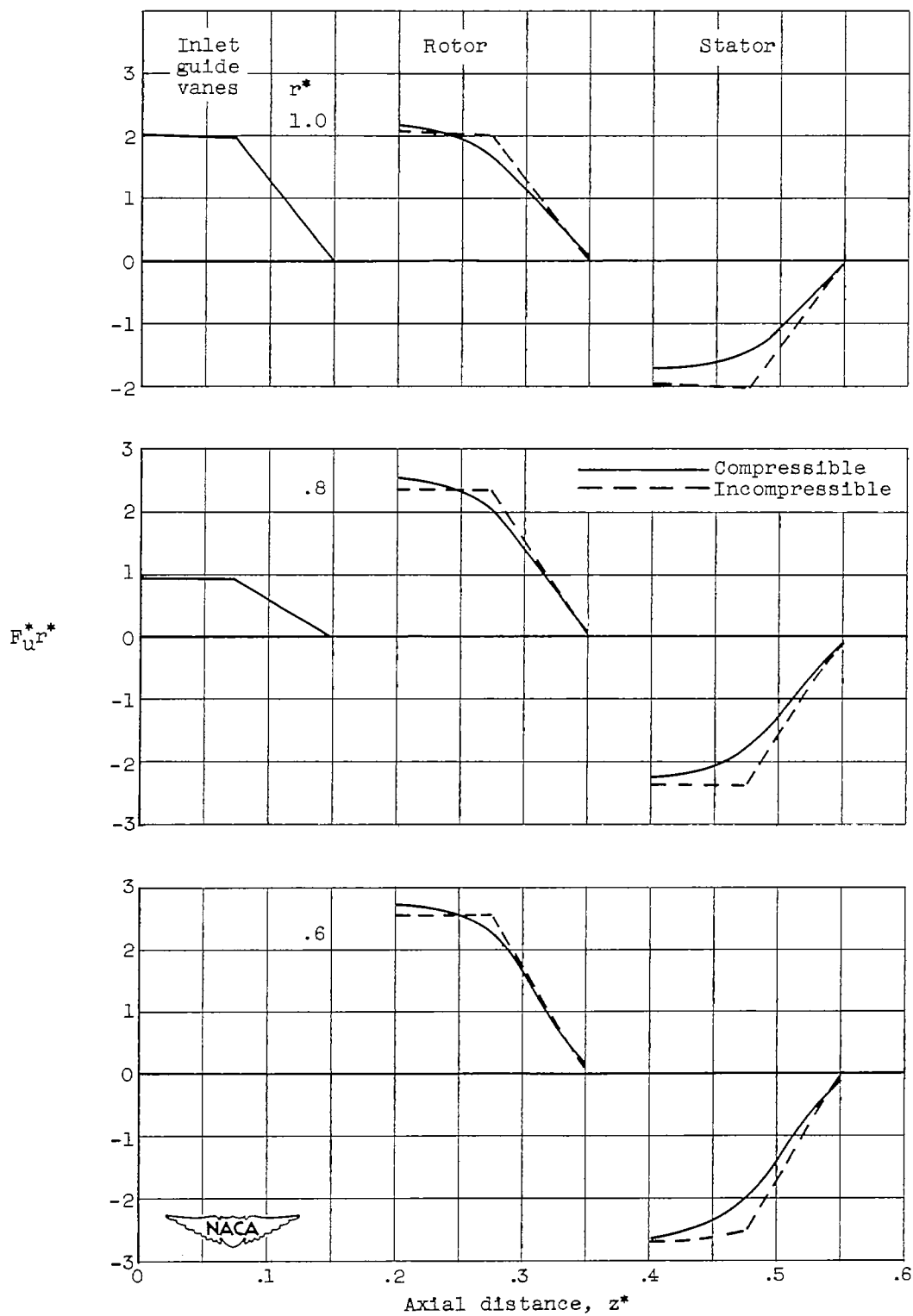
Figure 9. - Variation of $F_u^* r^*$.
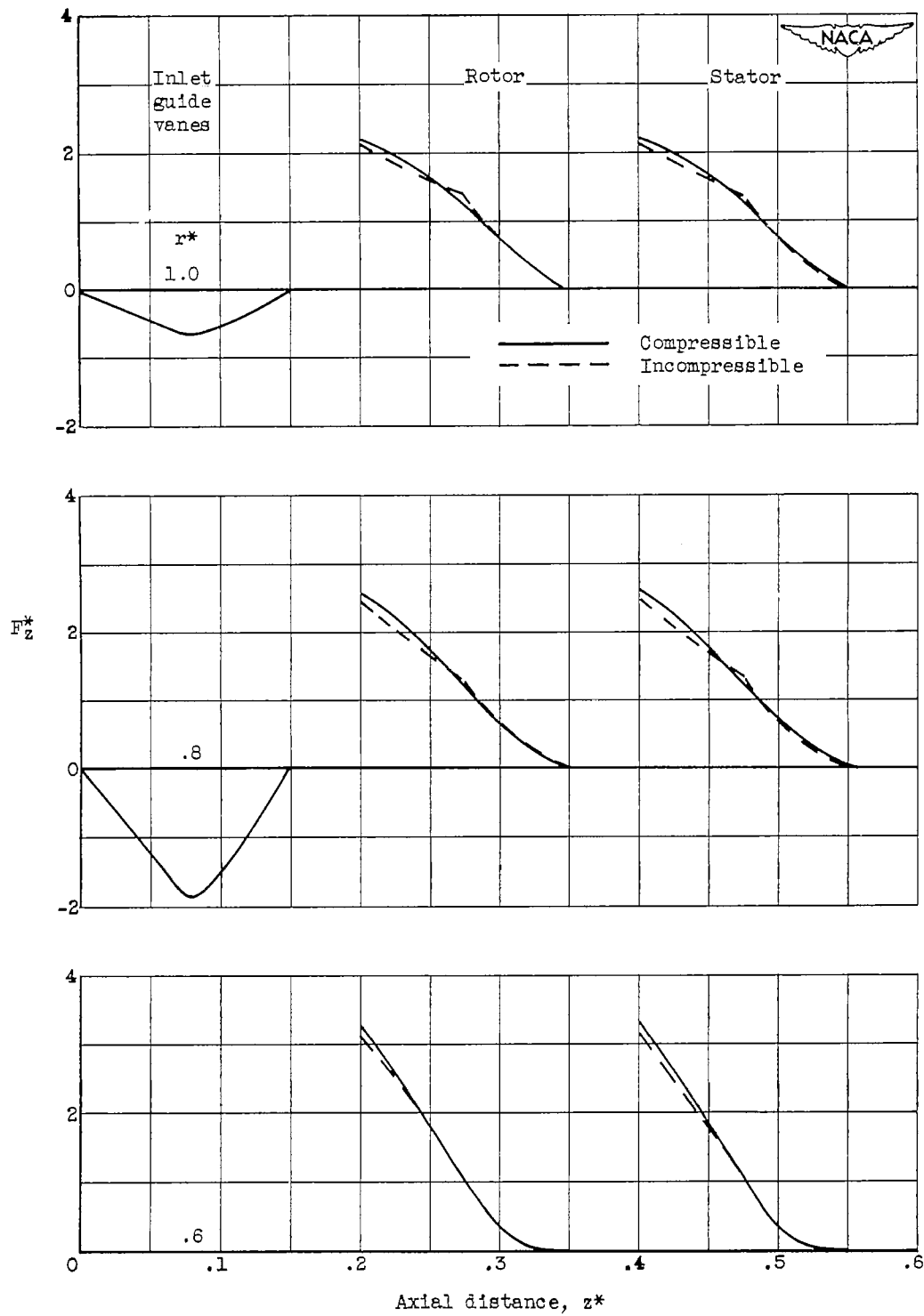
Figure 10. - Variation of F_z^*.
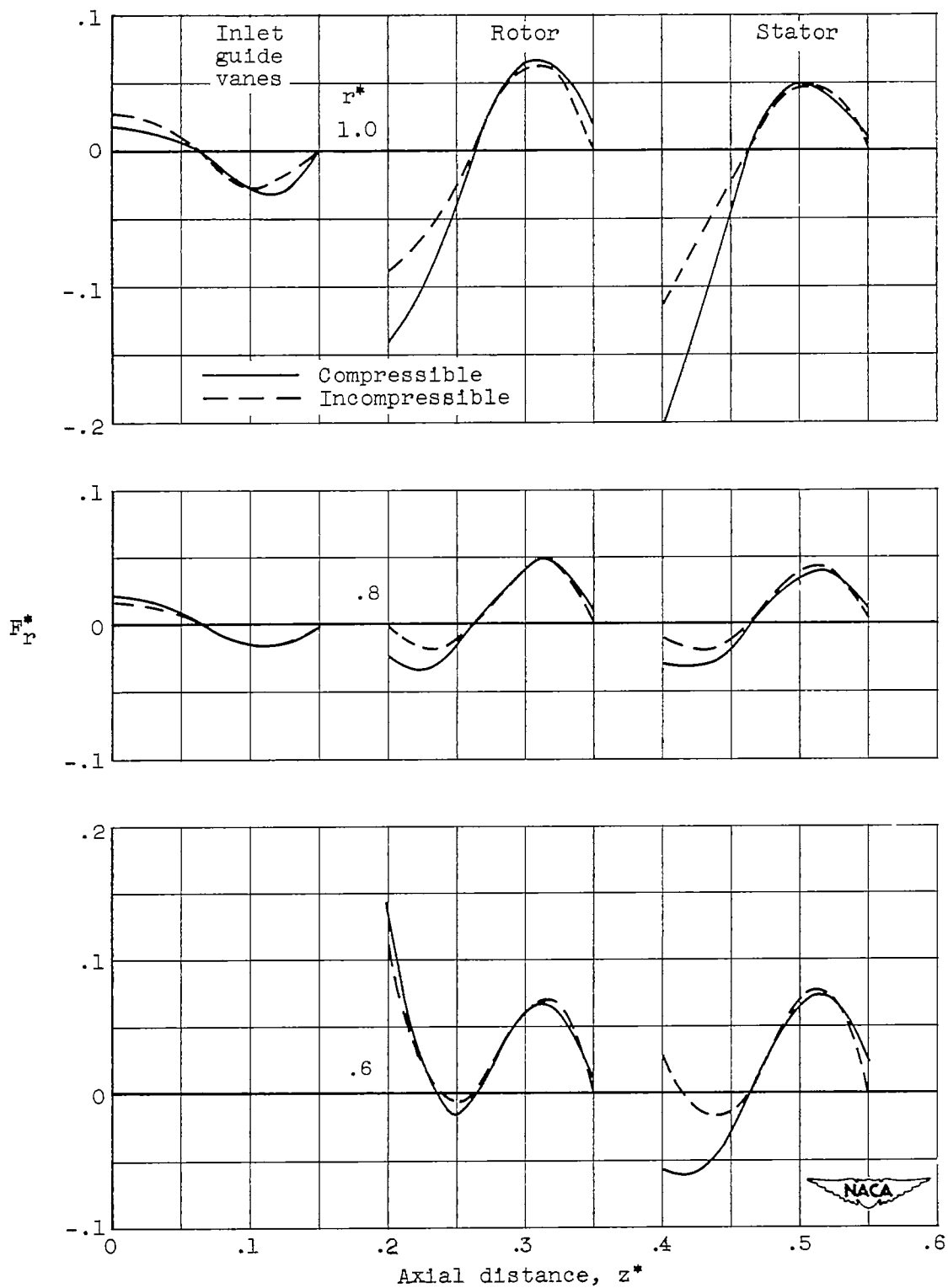
2519

Figure 11. - Variation of F_r^*.

(a) Axial distance $z^* = 0.175$.   (b) Axial distance $z^* = 0.375$.
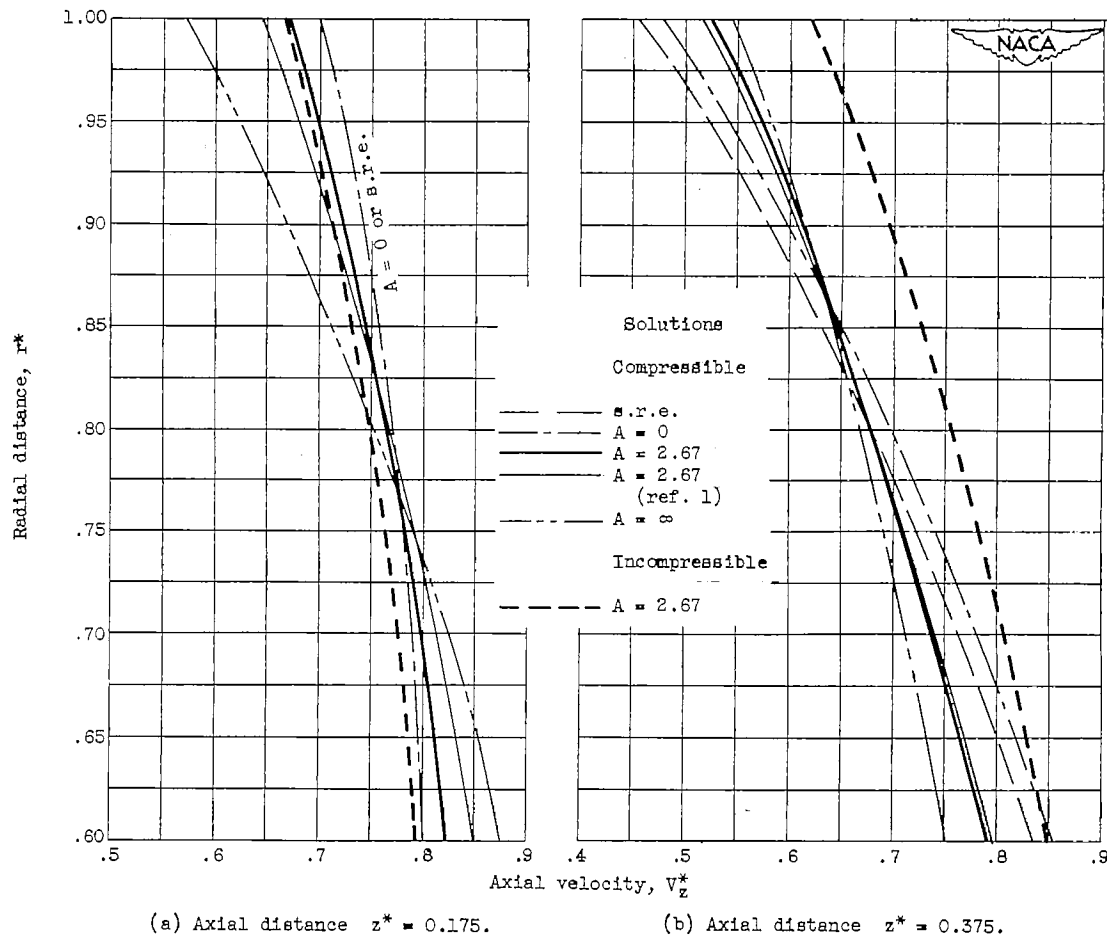
Figure 12. - Radial variation of axial velocity in front of and behind rotor. A, aspect ratio; s.r.e., simplified-radial-equilibrium.
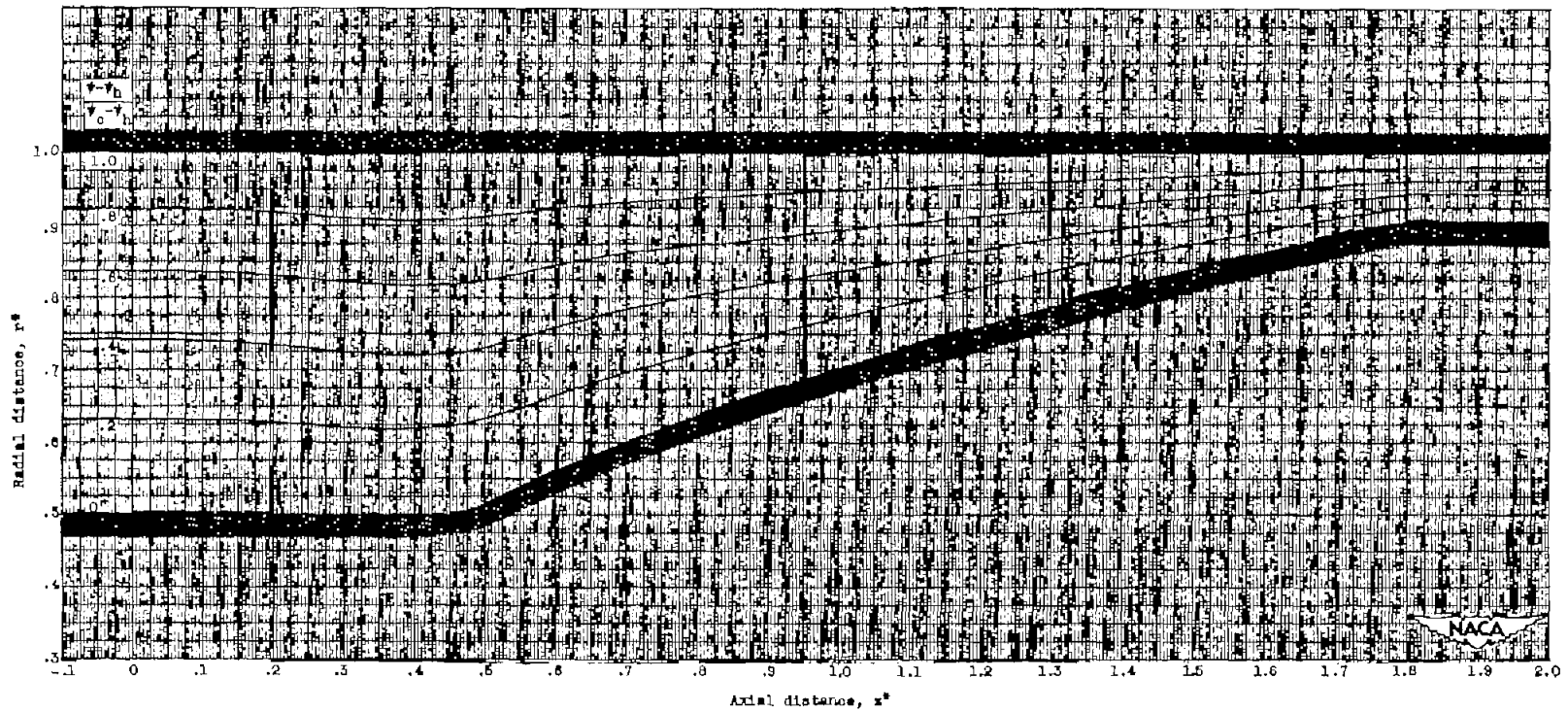
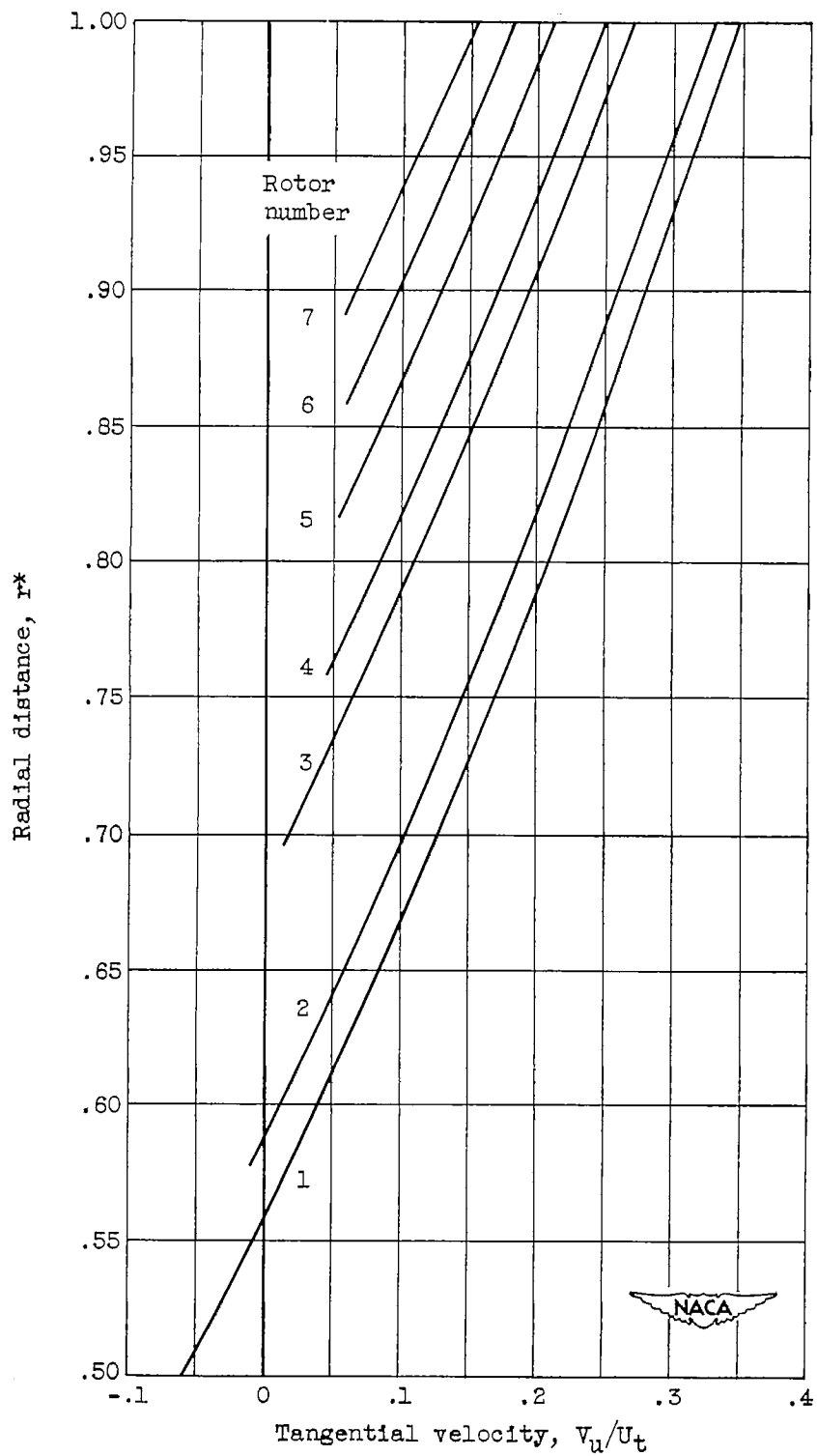Figure 13. - Meridional projection of compressible streamline in seven-stage compressor.

Figure 14. - Prescribed radial variations of tangential velocity at entrance to various rotors.